PCP
PLANT & CELL PHYSIOLOGY

Plasma Membrane Domains Participate in pH Banding of *Chara* Internodal Cells

Patric M. Schmölzer, Margit Höftberger and Ilse Foissner*

Department of Cell Biology, Division of Plant Physiology, University of Salzburg, 5020 Austria
*Corresponding author: E-mail, ilse.foissner@sbg.ac.at; Fax, +43-662-8044-619
(Received December 15, 2010; Accepted June 6, 2011)

Regular Paper

We investigated the identity and distribution of cortical domains, stained by the endocytic marker FM 1-43, in branchlet internodal cells of the characean green algae *Chara corallina* and *Chara braunii*. Co-labeling with NBD C_6-sphingomyelin, a plasma membrane dye, which is not internalized, confirmed their location in the plasma membrane, and co-labelling with the fluorescent pH indicator Lysotracker red indicated an acidic environment. The plasma membrane domains co-localized with the distribution of an antibody against a proton-translocating ATPase, and electron microscopic data confirmed their identity with elaborate plasma membrane invaginations known as charasomes. The average size and the distribution pattern of charasomes correlated with the pH banding pattern of the cell. Charasomes were larger and more frequent at the acidic regions than at the alkaline bands, indicating that they are involved in outward-directed proton transport. Inhibition of photosynthesis by DCMU prevented charasome formation, and incubation in pH buffers resulted in smaller, homogenously distributed charasomes irrespective of whether the pH was clamped at 5.5 or 8.5. These data indicate that the differential size and distribution of charasomes is not due to differences in external pH but reflects active, photosynthesis-dependent pH banding. The fact that pH banding recovered within several minutes in unbuffered medium, however, confirms that pH banding is also possible in cells with evenly distributed charasomes or without charasomes. Cortical mitochondria were also larger and more abundant at the acid bands, and their intimate association with charasomes and chloroplasts suggests an involvement in carbon uptake and photorespiration.

Keywords: Charasome • H^+-ATPase • Photosynthesis • Plant cell • Plasma membrane domain.

Abbreviations: AFW, artificial fresh water; BB, banding buffer; BSA, bovine serum albumin; CF, cytosolic fraction; CLSM, confocal laser scanning microscopy; DIC, differential interference contrast; DMSO, dimethylsulfoxide; EM, electron microscopy; FM 1-43, *N*-(3-triethylammoniumpropyl)-4-(dibutylamino)styryl pyridinium dibromide; FM 4-64, *N*-(3-triethylammoniumpropyl)-4-{6-[4-(diethylamino) phenyl] hexatrienyl}-pyridinium dibromide; MF, microsomal fraction; PBS, phosphate-buffered saline; TAPS, 3-{[Tris(hydroxymethyl) methyl]amino} propanesulfonic acid; TBST, Tris-buffered saline with Tween

Introduction

More than 40 years ago it was found that characean internodal cells are able to generate spatially separated bands of high and low pH in the medium adjacent to their cell surface (Spear et al. 1969, Lucas and Smith 1973). When exposed to light, the huge internodes show sharply peaked alkaline regions with pH values between 8.5 and 9.5, and more uniform acid regions with a pH of about 5.5. The pH bands disappear when photosynthesis is inhibited and the pH at the cell surface becomes uniform with values of about pH 6.0 (Lucas and Smith 1973). Different hypotheses have been proposed for the nature of this 'banding phenomenon'. Ion flux experiments showed that H^+ extrusion is localized in discrete bands along the cell length, apparently generated by H^+-ATPases, and that passive H^+ influx occurs predominantly at the alkaline regions (Spear et al. 1969, Lucas and Smith 1973, Spanswick 1981). Indeed, histochemical data suggest ATPase activity connected with plasma membrane chloride transport (Franceschi and Lucas 1982, Keifer et al. 1982, Price and Whitecross 1983). It has long been suggested that charasomes are involved in the pH banding pattern, and a pH-dependent distribution of these organelles has been reported (Franceschi and Lucas 1980, Price et al. 1985).

Charasomes are structured membrane elaborations along the longitudinal walls of internodal cells of the genus *Chara*, containing masses of anastomosing membranous tubules, surrounded by a continuous unit membrane (Barton 1965a, Barton 1965b, Crawley 1965). Histochemical data and detailed investigation of charasome development leave no doubt that the charasome membrane and plasma membrane are continuous (Franceschi and Lucas 1980, Lucas and Franceschi 1981). How the development of these structures is controlled has yet to be understood. *Chara corallina* grown in low pH media have

Plant Cell Physiol. 52(8): 1274–1288 (2011) doi:10.1093/pcp/pcr074, available online at www.pcp.oxfordjournals.org

fewer charasomes than those grown at alkaline pH (Price et al. 1985, Lucas et al. 1986), and inhibition of photosynthesis by either dark treatment or PSII-inhibiting drugs results in a complete but reversible loss of charasomes (Bisson et al. 1991, Chau et al. 1994). The function of charasomes has been the subject of speculation since they were first described. The tremendous increase in surface area between the cell and its environment indicates an involvement in transmembrane transport and, consequently, pH banding. More recent work on a pH-independent distribution of charasomes, however, has called this hypothesis into question (Bisson et al. 1991), which is supported by the fact that internodal cells of the genus *Nitella* display distinct pH banding patterns although they completely lack charasomes (Franceschi and Lucas 1980, Lucas and Franceschi 1981).

A close relationship between banding and photosynthesis has been confirmed by several studies showing enhanced photosynthesis at the acid regions in spite of a homogeneous distribution of chloroplasts (Lucas and Smith 1973, Plieth et al. 1994, Bulychev et al. 2001a, Bulychev and Vredenberg 2003). There is a broad consensus that the higher rates of photosynthesis at the acid regions are brought about by an enhanced availability of CO_2 after external conversion of HCO_3^- by a periplasmic carbonic anhydrase, but there also exist hypotheses about pH-dependent generation of bicarbonate or uptake of HCO_3^- (co-transport with protons) and internal conversion into CO_2 at either the acid or the alkaline regions of the cell (Ferrier 1980, Smith and Walker 1980, Walker et al. 1980, Lucas 1983, Price et al. 1985, Mimura et al. 1993, Chau et al. 1994, Ray et al. 2003). An involvement of charasomes in photosynthetic uptake of inorganic bicarbonate has been suggested (Price et al. 1985, Chau et al. 1994), but they have also been reported not to be essential for photosynthetic utilization of exogenous HCO_3^- (Lucas et al. 1989).

As a by-product of pH banding, characean cell walls calcify in the alkaline regions of their surface (Spear et al. 1969, McConnaughey and Falk 1991). These $CaCO_3$ encrustations, which can be more than half of the cells' dry weight, may either be formed by precipitation due to alkalization of the medium (Spear et al. 1969) or could involve active Ca^{2+} transport via Ca^{2+} ATPases (McConnaughey and Falk 1991).

In the present study we identified previously described fluorescently labeled cortical domains (Foissner and Klima 2008, Klima and Foissner 2008) as charasomes and show a clear correlation of their distribution with the pH banding pattern. Their involvement in banding activity was further confirmed by the localization of a plasma membrane-associated proton pump and by inhibitor experiments. The possibility to visualize charasomes in living *Chara* internodal cells opens up new perspectives for the study of plasma membrane elaborations and for the study of the plant plasma membrane H^+-ATPase which is of utmost importance for nutrient uptake, cell growth and intracellular pH homeostasis (Duby and Boutry 2008). The huge size and the cylindrical shape of the internodes allow surgical operations which make them a unique model for performing ion transport studies (Mimura 1995, Tazawa and Shimmen 2001, Tazawa 2003).

Results

For this work we used mainly internodal cells of *C. corallina* and *C. braunii*. The following results concerning plasma membrane staining, distribution of organelles, immunolabeling at the light and electron microscopic level and protein biochemistry pertain equally to both species. *Chara corallina* was preferred for in vivo imaging, immunofluorescence and protein biochemistry because of its nearly epiphyte-free cell walls and its rapid growth. However, its internodal cells are too long for high pressure freezing. Electron microscopic images presented in this study were therefore taken from *C. braunii*. Information about pH banding and staining results in *C. braunii* and *Nitella pseudoflabellata* is given in the **Supplementary material**.

Mapping of the pH banding pattern

Internodal cells of *C. corallina* (**Fig. 1A**), *C. braunii* (**Supplementary Fig. S1A**) and *N. pseudoflabellata* (**Supplementary Fig. S1D**) incubated in banding buffer (BB) containing phenol red showed clear banding patterns when exposed to light for several minutes (compare Spear et al. 1969). For this study we used internodal cells of the branchlets (shoots of limited growth; Wood and Imahori 1965) because of their 'smaller' size of up to 2 cm. These cells are better suited for light microscopic studies than the giant internodal cells of the main axis. We preferred young but non-elongating internodes because of their less developed $CaCO_3$ incrustations on their cell walls. These cells showed one to two alkaline regions, while older, more calcified internodes were separated into a greater number of alternating pH bands. Occasionally, the banding pattern showed circumferential irregularities. In this case the neutral line, which separates up- and downward streaming cytoplasm, formed the borderline between an acid and an alkaline region (arrow in **Fig. 1A**, compare with **Fig. 1F**). The previously reported mutability of the banding pattern of non-calcified cells (Lucas and Smith 1973, Fisahn and Lucas 1990, Bisson et al. 1991) could not be observed in this study and the positions of acid and alkaline bands remained stable for at least several hours.

Visualization of plasma membrane patches

The FM dyes such as FM 1-43 and FM 4-64 are anchored in the outer leaflet of the plasma membrane phospholipid bilayer before they are internalized via vesicular endocytosis (Betz et al. 1996). The plasma membrane of higher plant cells is evenly labeled by FM dyes (e.g. Bolte et al. 2004) but in *Chara* internodal cells FM dyes accumulated in conspicuous domains of the peripheral cytoplasm within a few minutes after incubation (**Fig. 1B–G**; **Supplementary Fig. S1A–C**; Klima and Foissner 2008). In young branchlet cells, as primarily used for

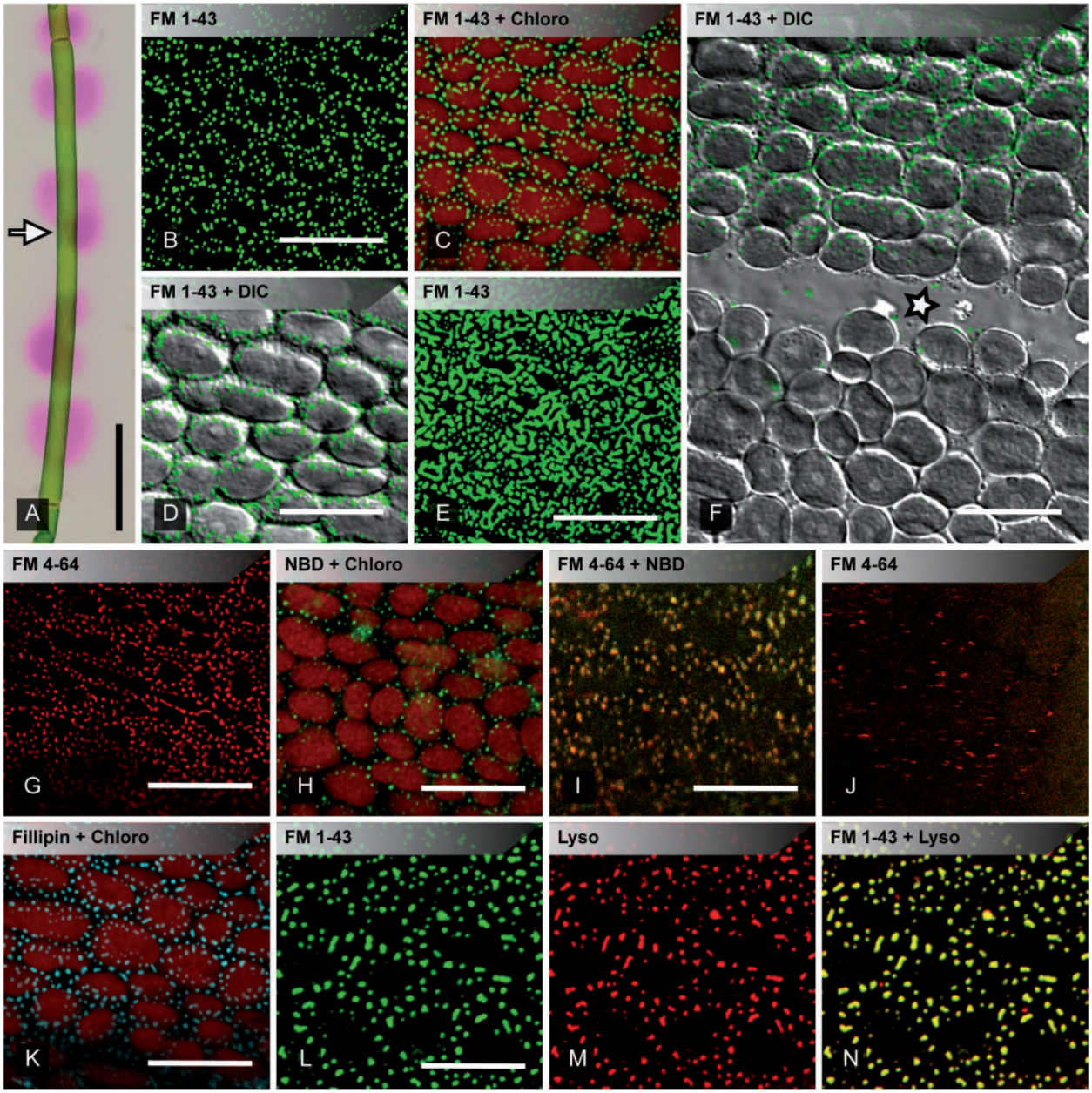

Fig. 1 pH banding and accumulation of lipophilic dyes in plasma membrane domains of *Chara corallina* internodal cells. (A) Alternating bands with high (pink) and low pH (slightly yellow) visualized with phenol red. Note the circumferential irregularity (arrow; compare with F). (B–F) FM 1-43-labeled plasma membrane domains. In young internodes FM patches (green) were round with diameters up to 1 μm (B) and were preferentially located between the stationary chloroplasts (C merged with red Chl autofluorescence and D merged with DIC). Highly branched meshworks were present in older internodes (E). (F) The neutral line (asterisk) occasionally formed the borderline between acid (upper part of the image) and alkaline regions (lower part of the image; compare with arrow in A). Note the heterogeneous distribution of FM patches (merged with DIC). (G and H) Plasma membrane domains stained with FM 4-64 (G) and with NBD C_6-sphingomyelin (H, merged with Chl autofluorescence. (I) Co-localization of NBD C_6-sphingomyelin- (green) and FM 4-64-stained plasma membrane domains (red). (J) In contrast to FM 4-64, NBD C_6-sphingomyelin was not internalized (J is a deeper optical section of the same cell shown in I). (K) Plasma membrane domains stained by filipin, a sterol-indicating dye. (L–N) Co-localization of FM 1-43 (L) and Lysotracker red (M, merged in N) suggests an acidic environment within these domains. Scale bars are 2 mm (A), 10 μm (D, I–J, L–N), 15 μm (F) and 20 μm (B–C, E, G, H, K).

this study, roundish patches with diameters up to 1 μm could be observed which were preferentially located at the periphery of the stationary chloroplasts (**Fig. 1C, D**). The cross-walls and the chloroplast-free neutral line were always free of FM-stained patches (**Fig. 1F**). In older, more calcified cells the FM-labeled cortical domains gained in complexity and formed a highly branched meshwork (**Fig. 1E**). These irregular complexes seemed to be restricted to acid bands, whereas alkaline regions of the same cell again showed discrete, round-shaped patches. However, detailed investigations of older cells turned out to be difficult, because of numerous autofluorescent precipitates and epiphytes on the cell walls. Membrane patches of young as well as older branchlet cells were larger and more frequent than those found in internodal cells of the main axis, and complex FM-labeled meshworks were never observed in internodes of the main axis (not shown).

Similar staining results were obtained with NBD C_6-sphingomyelin, a fluorescent sphingolipid which can be used for specific plasma membrane labeling (Grabski et al. 1993) although sphingomyelin does not exist in plants (Sebastien Mongrand, personal communication). The accumulation in patches was observed after 30 min incubation time (**Fig. 1H**), and double-staining with FM 4-64 revealed clear co-localization of both dyes in the same membrane domains (**Fig. 1I**). Unlike the FM dyes, NBD C_6-sphingomyelin remained in the plasma membrane and was not internalized, even after staining periods of up to 1 h. This was obvious in the streaming endoplasm of double-stained cells, where small FM-labeled vesicles without any signal of NBD C_6-sphingomyelin appeared (**Fig. 1J**). This finding implicating that the patches belong to the plasma membrane was confirmed by numerous co-localization studies using fluorescence markers and antibodies for different organelles such as mitochondria, lipid droplets and peroxisomes, since none of them co-localized with the patches (not shown; see also Klima and Foissner 2008). Staining with filipin, used as a specific marker for cholesterol in animal cells and sterol-like substances in plant cells (Grebe et al. 2003), was likewise restricted to the cell periphery, and internalization could not be observed with the equipment used in this study (**Fig. 1K**).

Neutral red, a lipophilic free base, has been commonly used for staining acidic organelles in living cells. Penetrating membranes in its unprotonated form and becoming trapped in acidic compartments due to protonation, this dye should be selective for environments with low pH, but is known to lack specificity (Dubrovsky et al. 2006). The acidotropic Lysotracker probes which consist of a fluorophore linked to a weak base are proposed to label acidic organelles with higher specificity, although their mechanism of retention has not been firmly established (Diwu et al. 1994). In lateral branchlet cells of *C. corallina*, both dyes, neutral red and Lysotracker red, accumulated within distinct plasma membrane domains, when incubated for 12 h at low light exposure in artificial fresh water (AFW; pH 5.5). Whereas neutral red showed high unspecific background fluorescence, membrane patches labeled with Lysotracker were easier to detect, due to a higher signal-to-noise ratio. Interestingly, both dyes were unable to stain plasma membrane patches when dissolved in a medium with higher pH (data not shown). Co-staining of branchlet cells with FM 1-43 and neutral red (not shown) or Lysotracker red (**Fig. 1L–N**), respectively, yielded clear co-localization in the plasma membrane domains, indicating an acidic environment.

In internodal cells of *N. pseudoflabellata*, FM-, NBD C_6-sphingomyelin- or filipin-stained plasma membrane domains were absent even when cells were incubated in BB for 14 d (**Supplementary Fig. S1D–F**).

Distribution of plasma membrane patches

Statistical analysis of the distribution of FM 1-43-stained patches along the longitudinal axis of lateral branchlet cells of *C. corallina* was performed on micrographs with an area of 2,500 μm^2, recorded in acid and alkaline bands. Serial optical sections (Z-series) were used for projections, to capture as much surface area as possible.

Typical views of such micrographs are shown in **Fig. 2B and C**, representing plasma membrane domains in an acid band and an alkaline band (compare with **Fig. 2A**). The acid bands showed abundant roundish, elongate or irregularly shaped FM-stained domains which had an average size of about 0.7 μm^2 (**Fig. 2B, D**). Less and smaller, mostly punctate plasma membrane domains were observed in alkaline regions (**Fig. 2C, D**). Furthermore, membrane domains in acid regions always showed higher fluorescence intensities as compared with those in alkaline bands of the same cell, using similar settings for laser intensity, detector gain and pinhole diameter (insets in **Fig. 2B and C**). To compile statistics on membrane domain distribution, 102 micrographs (51 images from each region) from 13 internodal cells were examined corresponding to a total surface area of 127,500 μm^2. The distribution of data was non-normal as determined by the Kolmogorov–Smirnov test. Box-and-whisker plots were therefore used to show median values for size, density and area fraction (**Fig. 2D–F**). A non-parametric test, the Mann–Whitney rank sum test (U-test), confirmed that plasma membrane patches were significantly smaller and less abundant in alkaline bands than in acid regions. Therefore, FM-stained domains occupied about 13% of the cell surface at acid regions but <2% at the alkaline bands.

The non-normal distribution of FM-labeled patches in different branchlet cells could be attributed to differences in cell age with different development stages of plasma membrane domains. Indeed, examination of patch distribution only of bands which had been investigated from the same cell resulted in normal distributions in all branchlet cells. The pair-wise comparison of the size, the density and the area fraction in acid and alkaline bands of three cells is shown in **Table 1**. Here, the parametric Student's *t*-test again showed significant differences in size and abundance of patches between acid and alkaline bands of the same cell.

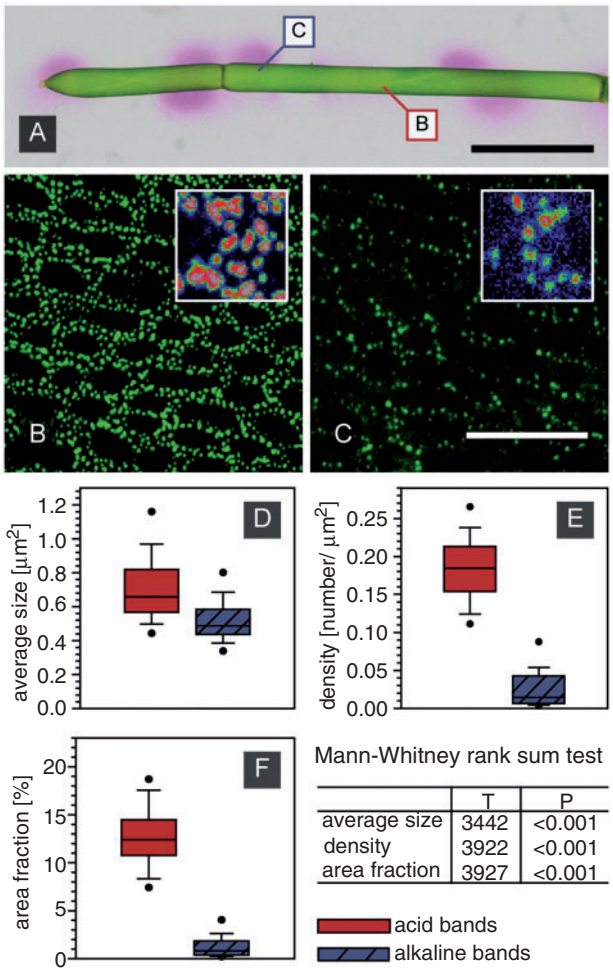

Fig. 2 Distribution of membrane patches correlates with pH banding. (A) Banding pattern of two internodes visualized with phenol red. Alkaline bands are indicated by pink regions. Captions indicate regions shown in B and C. (B and C) Membrane patches labeled with FM 1-43 were apparently larger and more abundant within acid bands (B) than in alkaline regions (C). Additionally, patches in acid bands showed brighter fluorescence signals compared with those in alkaline bands (insets in B and C). (D–F) Average size (D), density (E) and area fraction (F) are compared in box-and-whisker plots. Shown are median values with upper and lower quartiles (box), largest and lowest non-outlier observations (whiskers), as well as 5th and 95th percentiles (dots) with $n = 51$ for each band. Differences between median values of acid and alkaline bands (D–F) are significant. Scale bars are 2.5 mm (A) and 20 µm (B and C).

pH banding-dependent size and differential distribution of plasma membrane domains were also observed in internodal cells of *C. braunii* (**Supplementary Fig. S2A–C**).

Detection and localization of a plasma membrane proton pump

To support further the hypothesis that FM-stained membrane domains participate in pH banding, we analyzed the distribution of a plasma membrane proton pump using an antibody against plasma membrane ATPase.

Table 1 Pair-wise comparison (Student's *t*-test) of the average size, the density and the area fraction of FM-labeled plasma membrane domains of pH bands from the same cell

Cell no.	Acid bands	Alkaline bands	*t*	*P*
Average size (µm²)				
1	0.60 ± 0.08	0.50 ± 0.03	3.060	0.012
2	0.68 ± 0.08	0.45 ± 0.10	4.474	0.001
3	1.02 ± 0.04	0.69 ± 0.03	2.663	0.024
Density (number per µm²)				
1	0.21 ± 0.06	0.04 ± 0.02	6.311	<0.001
2	0.19 ± 0.02	0.03 ± 0.01	15.975	<0.001
3	0.18 ± 0.03	0.01 ± 0.01	11.616	<0.001
Area fraction (%)				
1	12.14 ± 2.16	1.86 ± 0.77	10.990	<0.001
2	13.05 ± 1.75	1.09 ± 0.46	16.197	<0.001
3	17.45 ± 2.16	0.46 ± 0.44	18.914	<0.001

Data are given as mean ± SD with $n = 6$.

This antibody recognized a prominent, distinct band of about 100 kDa in protein extracts of microsomal fractions of *C. corallina* and a weaker band in the lower molecular mass range (**Fig. 3A**). To check whether the additional signal at about 30 kDa is due to unspecific binding properties or is caused by protein degradation, a second approach without the use of protease inhibitors during sample preparation was carried out. In this case a strong labeling in the 30 kDa range could be detected, whereas only a weak signal was observed at 100 kDa. This suggests that the 30 kDa bands are due to protein degradation and proves a high specificity for the antibody–antigen reaction.

The same antibody used for immunofluorescence of internodal cells revealed a heterogeneous distribution of the proton ATPase correlating with that of plasma membrane domains stained with the fixable analog of FM 1-43 (**Fig. 3B, C**). The overlay image as well as the line plot revealed clear co-localization (**Fig. 3D, E**). After background subtraction of the antibody signal, co-localization rates up to 98.3% (Pearson's correlation up to 0.86) were obtained and quantified by scatter plots.

Fig. 3F shows an electron micrograph of a section from a high pressure frozen and cryosubstituted *C. braunii* internodal cell. Smooth plasma membrane regions alternate with convoluted domains, the charasomes, which are often located in close proximity to cortical chloroplasts and mitochondria. Immunolabeling with the antibody against plasma membrane H^+-ATPase revealed accumulation of gold beads at charasomes and scattered gold beads at smooth plasma membrane regions and at the cell wall (**Fig. 3G, H**). On sections incubated with pre-immune serum instead of the primary antibody, charasomes and smooth plasma membrane regions were not or only occasionally labeled. The cell wall was still covered by obviously unspecifically bound gold beads (**Fig. 3I**).

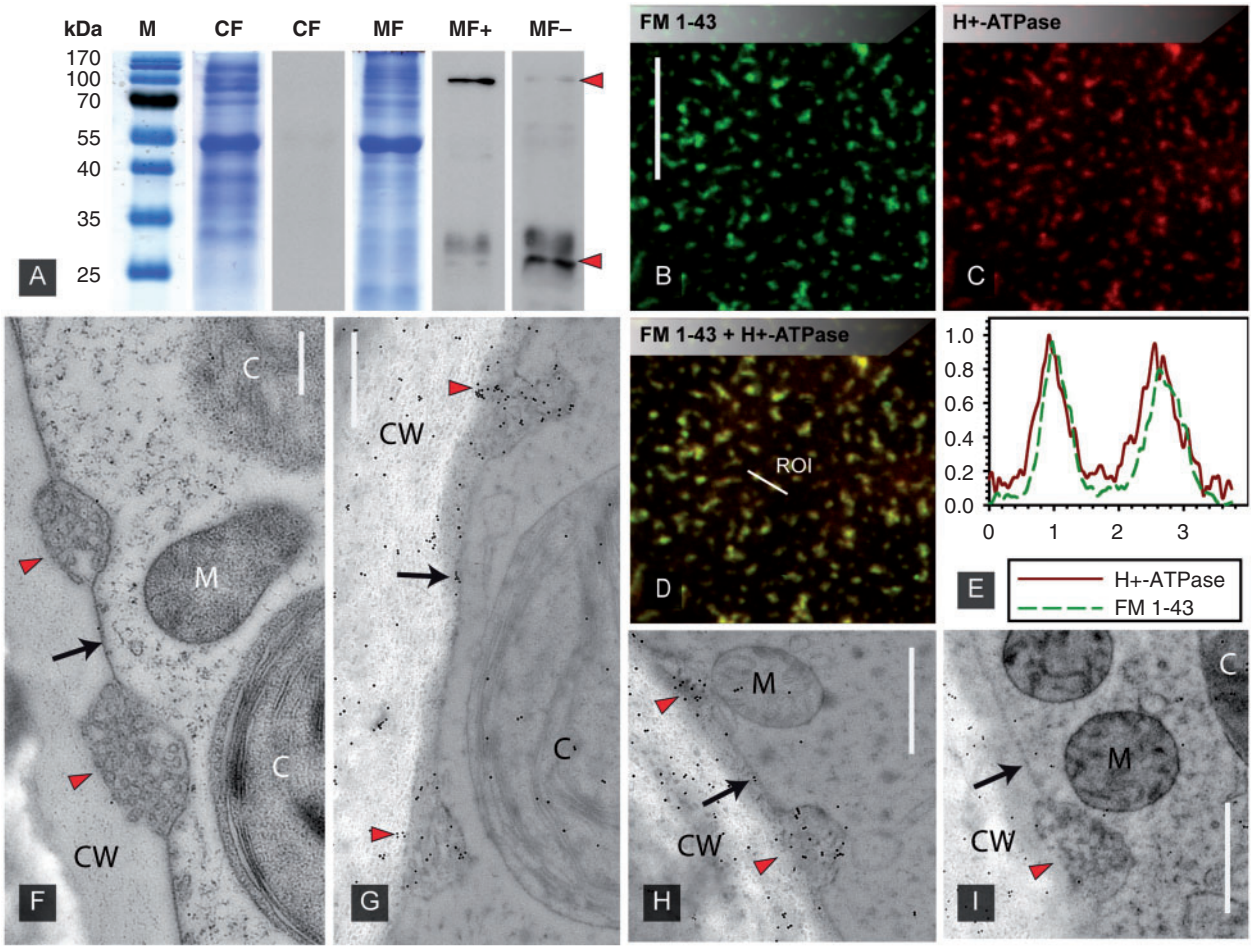

Fig. 3 Western blot analysis and immunolocalization using an antibody against plasma membrane H^+-ATPase. (A) Cytosolic (CF) and microsomal fractions (MF) were separated on 10% SDS gels. The antibody recognized a 100 kDa band in the MF (MF+, upper arrowhead). The smaller signal at about 30 kDa (lower arrowhead) is strongly enhanced in samples prepared without protease inhibitors (MF−) suggesting protein degradation. (B–E) FM 1-43 fluorescence (B) and immunofluorescence of the plasma membrane proton pump (C). The merged image (D) as well as line plots (E with the distance in μm on the *x*-axis and relative fluorescence values on the *y*-axis corresponding to the line ROI in D) show clear co-localization. (F–I) Immunogold labeling of the plasma membrane proton pump on EM sections. Charasomes (red arrow heads) are visible between smooth plasma membrane regions (black arrows). Unstained control section (F), immunolabeling with first and second antibody (G and H) and negative control with pre-immune serum instead of first antibody (I). Note the accumulation of gold beads in charasomes and unspecific labeling of the cell wall (CW). C, chloroplast; M, mitochondrion. Scale bars are 10 μm (B–D) and 500 nm (F–I).

Taken together, our data obtained by immunofluorescence and immunogold labeling suggest that the fluorescently labeled plasma membrane domains correspond to charasomes and that they harbor a H^+-ATPase which possibly mediates their involvement in pH banding.

Effects of the photosynthetic inhibitor DCMU

It has been reported that inhibition of photosynthesis by dark treatment or drugs results in a complete loss of charasomes (Bisson et al. 1991, Chau et al. 1994). We therefore applied DCMU, an inhibitor of PSII, to investigate the effects of photosynthesis on the morphology of fluorescently stained plasma membrane domains and to confirm further that they are identical to charasomes. Application of DCMU resulted in a nearly immediate, complete loss of the pH banding pattern (**Fig. 4A, B**) but had no effect on cytoplasmic streaming, which is another prerequisite for pH banding (Lucas and Dainty 1977, Bulychev et al. 2001b). Streaming continued at control rates over the duration of the experiment (not shown), whereas FM patches underwent massive degradation (**Fig. 4C–E**). A first decrease in patch size and density measured at the acid regions could already be seen after 2 d of incubation. After 10 d all patches had completely disappeared so that the plasma membrane was almost homogenously labeled. In contrast, control cells incubated in BB showed a steady increase in the area covered by FM patches until a complex network was present at the cell surface after 10 d (compare **Fig. 1B**).

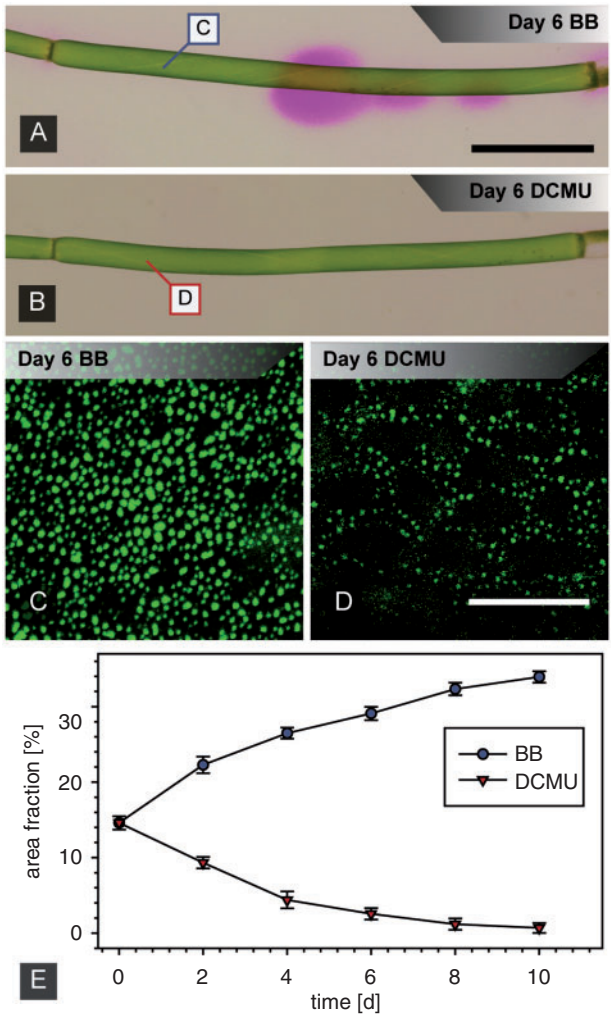

Fig. 4 Effects of the photosynthesis inhibitor DCMU on pH banding (A and B) and FM-labeled plasma membrane domains (C–E). (A and B) pH banding (A, control cell in banding buffer BB) is abolished in the presence of DCMU (B). Insets mark the position of images C and D. (C and D) FM-stained plasma membrane domains of internodes incubated in BB (C) or in DCMU (D) for 6 d. (E) Time course of area fraction of FM-labeled plasma membrane domains at the acid regions of control cells incubated in BB buffer and in DCMU-treated cells, respectively. Data are given as means ± SEM ($n = 6$ from three cells). Scale bars are 1.5 mm (A and B) and 20 µm (C and D).

Effects of pH buffers

The differential distribution of charasomes according to the pH banding pattern could be caused by extreme changes in extracellular pH, and the degradation (or non-development) of charasomes in DCMU-containing solutions could be the indirect effect of inhibition of pH banding. We therefore studied the effect of extracellular pH on the size and distribution of charasomes using 5 mM MES, HEPES and TAPS to clamp the pH of the BB at 5.5, 7 (intermediate data not shown) and 8.5, respectively. This treatment resulted in an immediate loss of banding, and the pH at the surface of the internodal cells became uniform (**Fig. 5A, G**). As controls we used cells incubated in BB with the same pH adjusted with HCl or KOH but without MES, HEPES or TAPS. These cells were still able to generate acid and alkaline bands (not shown). The addition of pH buffers profoundly affected the size and distribution of FM-stained plasma membrane domains. After 6 d treatment plasma membrane domains at the (previously) acid bands were significantly smaller than those of the controls and had a similar size irrespective of whether the pH of the BB was clamped at 5.5 with MES (**Fig. 5B–D**; **Table 3**) or at 8.5 with TAPS (**Fig. 5H–J**; **Table 3**). At pH 8.5 a significant decrease in density was also noted at the acid bands (**Fig. 5K**; **Table 3**). Charasome size and density at the alkaline bands were less affected. Therefore, average size, density and area fraction of the FM-stained patches became similar at the previously acid and alkaline bands, and differences between means were statistically not significant (see Mann–Whitney rank sum tests in **Fig. 5**). In the controls (BB 5.5 and BB 8.5) significant differences between acid and alkaline bands were observed (Mann–Whitney rank sum tests in **Fig. 5**; compare with **Fig. 2**).

As outlined above, all pH buffers caused inhibition of pH banding and a homogeneous distribution of similarly sized plasma membrane domains irrespective of the pH value. In actively banding cells, however, the size and density of FM-labeled plasma membrane domains at the acid bands varied according to the pH of the medium. Under the experimental conditions applied in this study, FM-stained plasma membrane domains at the acid bands of cells incubated in BB 5.5 were significantly larger than plasma membrane domains at the acid bands of cells incubated in BB 8.5 ($P = 0.016$; **Fig. 5D, J**). The density at the acid regions, however, was significantly lower in BB 5.5 as compared with BB 8.5 ($P < 0.001$; **Fig. 5E, K**) which resulted in similar, not significantly different area fractions (**Fig. 5F, L**). This indicates that in our experiments an alkaline pH favored the formation of smaller but more numerous plasma membrane domains at the acid regions of actively banding cells. Plasma membrane domains at the alkaline bands were not significantly affected by the pH of the BB (compare **Fig. 5D–F** with **J–L**).

The above described data appear to reflect a steady state because similar results for average size, density and area fractions were obtained in cells treated with BB ± pH buffers for 18 d (not shown). FM-labeled patches were never completely lost as observed after 10 d treatment with DCMU.

Visualization and distribution of cortical mitochondria

We have previously reported that mitochondria are larger and more abundant at the acid regions of internodal cells compared with the alkaline sites (Foissner 2004). In this study we compared their distribution with that of the charasomes. Mitotracker orange is a fluorescent dye that stains mitochondria in living cells. It can be used to monitor the mitochondrial

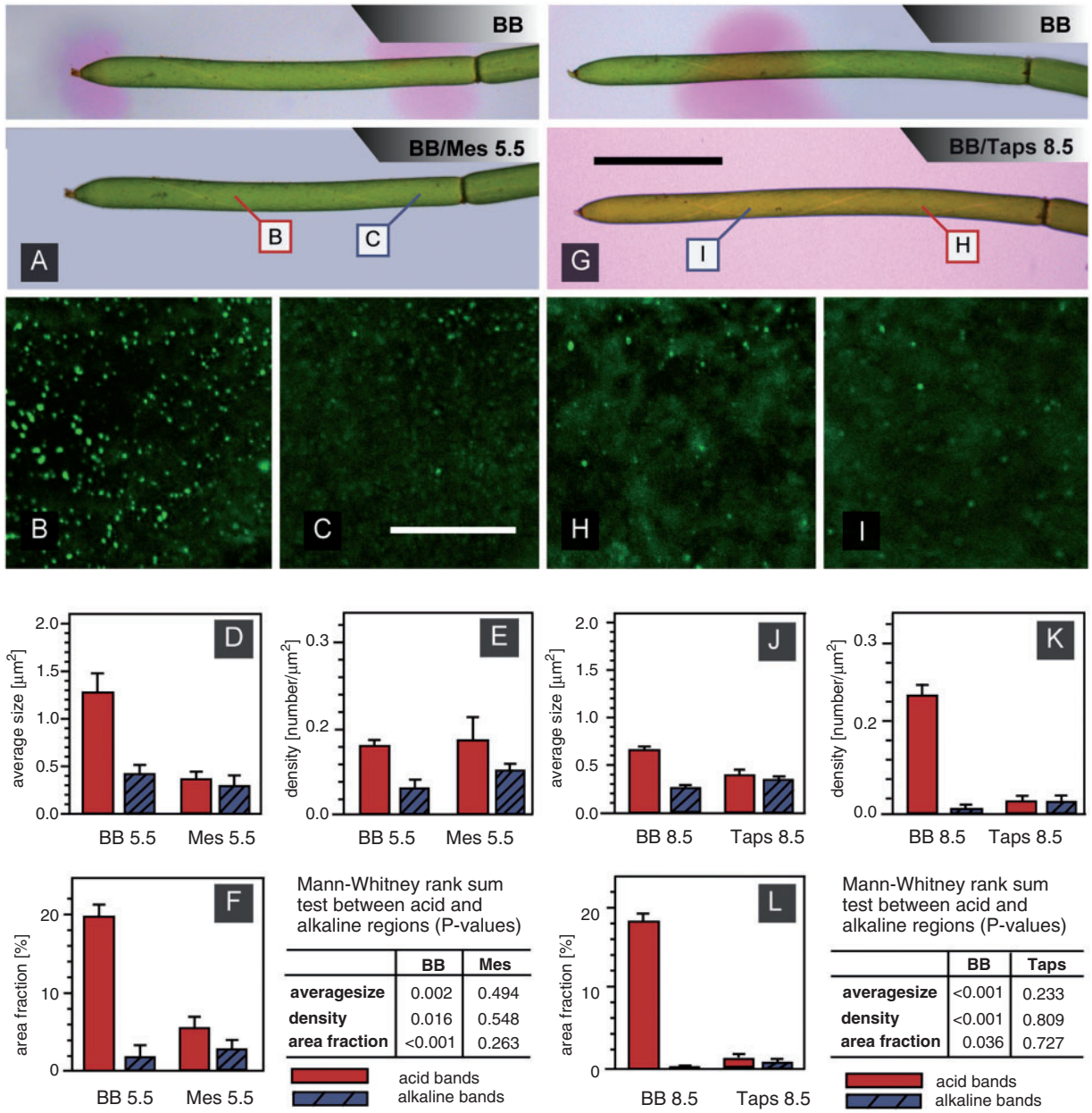

Fig. 5 Effects of pH buffers on pH banding (A and G) and size and distribution of FM-labeled plasma membrane domains (B–F and H–L). (A) pH banding pattern in BB and after addition of 5 mM MES, pH 5.5. Insets mark the positions of images B and C. (B and C) FM-labeled plasma membrane domains at a previously acid (B) and alkaline region (C) of a cell treated with BB + 5 mM MES, pH 5.5 for 6 d (compare with **Fig. 2B and C**). (D–F) Comparison of average size (D), density (E) and area fraction (F) of FM-labeled plasma membrane domains of cells treated with BB, pH 5.5 and BB + 5 mM MES, pH 5.5, respectively. Data are given as means ± SEM from six cells; differences between acid and alkaline regions are significant in BB only. (G) pH banding pattern in BB and after addition of 5 mM TAPS, pH 8.5. Insets mark the positions of images H and I. (H and I) FM-labeled plasma membrane domains at a previously acid (H) and alkaline region (I) of a cell treated with BB + 5 mM TAPS, pH 8.5 for 6 d. (J–L) Comparison of average size (J), density (K) and area fraction (L) of FM-labeled plasma membrane domains of cells treated with BB, pH 8.5 and BB + 5 mM TAPS, pH 8.5, respectively. Data are given as means ± SEM from six cells; differences between acid and alkaline regions are significant in BB only. Scale bars are 2.5 mm (A, G) and 20 µm (B and C, H and I).

membrane potential, due to its membrane potential-dependent accumulation (Zhang et al. 1994). In the internodes used in this study, mitochondria mostly had a bean-like appearance with a length of up to 2 µm and were larger in size than the FM-labeled membrane domains (**Supplementary Fig. 2B, G, H**; compare Foissner 2004). Differences in the distribution of mitochondria between acid and alkaline bands were obvious (**Supplementary Fig. S2A–C**). Data were normally distributed,

and parametric Student's *t*-test confirmed that mitochondria were significantly smaller and fewer in alkaline bands, resulting in highly significant differences in area fraction (**Table 2**; **Supplementary Fig. S2D–F**; compare Foissner 2004). Cortical mitochondria were closely associated with FM 1-43-stained plasma membrane domains and nestled between the stationary plastids (**Supplementary Fig. S2G, H**). Mitochondria in alkaline regions were more weakly stained than those in acid bands of the same cell, suggesting differences in mitochondrial membrane potential (insets in **Supplementary Fig. S2B, C**).

To summarize, membrane patches and mitochondria were significantly more frequent in the acid bands than in alkaline regions.

Discussion

The charasome complex as a target of dye accumulation

We have shown previously that FM dyes stain discrete domains (patches) in the periphery of characean internodal cells (Klima and Foissner 2008). Here we used different markers for in vivo imaging, immunofluorescence and immunogold labeling, as well as inhibitor experiments in order to unravel their identity and to elucidate their physiological function. The use of NBD C_6-sphingomyelin as a plasma membrane-specific fluorescence probe (Grabski et al. 1993) and various co-localization studies (Klima and Foissner 2008, this work) leave no doubt that these structures belong to the plasma membrane.

Likely targets of dye accumulation are charasomes, whose complex membrane invaginations offer enough binding sites for lipophilic dyes. Both morphology and development of membrane patches are consistent with electron microscopy (EM) observations which showed that charasomes start with small (up to 1 μm) disc-like domains in young internodes and form highly irregular complexes in older cells (Franceschi and Lucas 1980). As reported for charasomes, these patches were apparently larger and more frequent in internodes of branchlets than in internodal cells of the main axis and they were absent from cross-walls and from the neutral line (Franceschi and Lucas 1980). The most obvious evidence for their identity is given by direct correlation of fluorescence labeling with EM observations, using an antibody against a H^+-ATPase. While immunofluorescence showed a clear co-localization with the FM-stained patches, immunogold labeling of EM sections revealed an accumulation within the charasome complex.

The FM-labeled cortical domains are also stained by filipin, a sterol-specific marker (Robinson and Karnovsky 1980), and we previously suggested that these patches represent clusters of lipid rafts (Foissner and Klima 2008). In view of the data presented here, it is, however, possible that the filipin staining does not reflect an accumulation of sterols, but merely a local increase in superimposed plasma membrane material as found in charasomes, due to their convoluted membranous structure. The local increase in plasma membrane material could also account for the intense labeling of charasomes by the antibody against the H^+-ATPase which, in contrast to earlier findings (e.g. Mongrand et al. 2004), has recently been shown not to be enriched in lipid rafts or fractions of detergent-insoluble membranes, respectively (Raffaele et al. 2009).

Alternating bands of acid and alkaline pH have also been reported from internodal cells of various *Nitella* species which lack charasomes and have a smooth plasma membrane

Table 2 Distribution of cortical mitochondria

Mitochondria ($n = 39$)	Acid bands	Alkaline bands	*t*	*P*
Average size (μm²)	1.78 ± 0.34	1.20 ± 0.23	8.822	<0.001
Density (number per μm²)	0.06 ± 0.01	0.03 ± 0.01	14.850	<0.001
Area fraction (%)	10.52 ± 1.63	3.51 ± 1.34	20.810	<0.001

All data are given as mean ± SD. Samples were compared with parametric Student's *t*-test, as all data showed normal distribution examined with the Kolmogorov–Smirnov test.

Table 3 Effect of pH buffering on the average size, the density and the area fraction of FM-labeled plasma membrane domains at (previously) acid and alkaline pH bands

	BB 5.5	MES 5.5	*P*	BB 8.5	TAPS 8.5	*P*
Average size (μm²)						
Acid bands	1.26 ± 0.19	0.38 ± 0.05	0.004	0.68 ± 0.03	0.40 ± 0.05	<0.001
Alkaline bands	0.43 ± 0.06	0.31 ± 0.08	NS	0.27 ± 0.01	0.34 ± 0.02	0.024
Density (number per μm²)						
Acid bands	0.16 ± 0.01	0.17 ± 0.05	NS*	0.27 ± 0.02	0.03 ± 0.01	<0.001
Alkaline bands	0.06 ± 0.02	0.10 ± 0.03	NS	0.01 ± 0.00	0.03 ± 0.01	NS
Area fraction (%)						
Acid bands	19.33 ± 1.68	5.06 ± 1.88	<0.001	18.35 ± 0.87	1.17 ± 0.45	<0.001
Alkaline bands	1.88 ± 1.09	2.74 ± 0.87	NS	0.30 ± 0.10	0.96 ± 0.25	NS*

Cells were incubated in BB ± 5 mM MES or TAPS, respectively. Data are means ± SEM from six cells; *P*-values were obtained by Student's *t*-test (normal distribution of data) or by Mann–Whitney rank sum test* (non-normal distribution of data). For differences **between** acid and alkaline regions see **Fig. 5**.

according to EM observations (Lucas and Franceschi 1981, who investigated *N. translucens*, and the authors' own unpublished data from *N. flexilis*, *N. hyalina* and *N. pseudoflabellata*). The absence of charasomes in *Nitella* is supported by our staining results obtained with internodal cells of *N. pseudoflabellata* which were incubated in BB for 14 d. Neither FM 1-43, NBD C_6-sphingomyelin nor filipin labeled plasma membrane domains comparably with those in *Chara* internodes. The previously mentioned FM-stained plasma membrane domains in *Nitella* (Foissner and Klima 2008) probably represented epiphytes which are always heavily stained by fluorescent dyes. Therefore, pH banding in *Nitella* internodal cells is due either to differential activation of proton ATPases or to functionally but not morphologically specialized plasma membrane domains which may concentrate transmembrane transport elements.

Differential distribution of charasomes is correlated with pH banding in undisturbed cells

Early EM studies already suggested a distinct relationship between charasomes and pH banding. They were reported to be larger and more frequent in acid bands (Franceschi and Lucas 1980), which was later confirmed by statistical analysis (Price et al. 1985). In contrast to these data, Bisson et al. (1991) could not find any correlation between charasomes and pH bands. Other arguments also called such a relationship into question. First, internodal cells of the genus *Nitella* are able to generate pH banding patterns although they completely lack charasomes (see above). Secondly, the banding pattern of young, non-calcified internodes has been reported to be quite changeable, being affected by dark, pH of the medium and other perturbations, which argues against a participation of the more stable charasomes (Fisahn and Lucas 1990, Bisson et al. 1991, Bulychev et al. 2001a, Bulychev et al. 2001b). Thirdly, pH banding is re-established before measureable charasome recovery after complete loss due to inhibition of photosynthesis (Chau et al. 1994) or treatment with pH buffers (this study). These data confirmed that the ability to band indeed does not necessarily require charasomes, but participation or an enhancement of banding activity cannot be ruled out.

In this study, using internodal cells of the branchlets, we found a distinct correlation between pH banding and the distribution of charasomes, which were significantly larger and more frequent within the acid bands than at alkaline regions. Furthermore, FM-labeled membrane patches in acid bands were always characterized by brighter fluorescence, indicating that charasomes of alkaline bands are less complex in their structure and, therefore accumulate less lipophilic dyes. It is possible that the contradictory data concerning a relationship between charasomes and pH banding are due to the use of different cells. Bisson et al. (1991) who could not find any correlation used internodes of the main axis and not internodes of branchlets, as investigated here and in the study of Price et al. (1985). In internodal cells of the main axis the banding pattern appears to be quite changeable, especially in young cells which do not have precipitated $CaCO_3$ known to stabilize the alkaline regions (Fisahn and Lucas 1990). Charasomes (Franceschi and Lucas 1980) and FM-stained membrane patches (data not shown) are smaller and fewer in internodal cells of the main axis than in internodal cells of the branchlets. It can thus be postulated that charasomes of branchlet cells show a higher grade of structural as well as functional development which could serve to amplify the capacity for transmembrane fluxes of important substances. This is consistent with the finding that internodal cells of the main axis have a less important role in photosynthesis than the branchlets (Schulte et al. 1994). Whether the development of charasomes and the pH banding is a prerequisite for local differences in the rate of photosynthesis or a secondary event remains to be investigated (Bulychev and Vredenberg 2003).

Involvement of charasomes in external acidification

Our data support the hypothesis that charasomes are involved in active medium acidification caused by the activity of a H^+-ATPase (Franceschi and Lucas, 1982, Price and Whitecross 1983). In this study we used an antibody raised against a synthetic peptide derived from various higher plant and algal plasma membrane ATPase sequences including those of *Arabidopsis thaliana* (Harper et al. 1989) and *Chlamydomonas reinhardtii* (Campbell et al. 2001). The antibody showed a strong and highly specific cross-reaction in the appropriate 100 kDa range in Western blot analysis, and immunolocalization revealed an accumulation of proton pumps within charasomes, confirming the idea of active acidification mediated through charasome-associated H^+-ATPase activity in acid bands. These findings are consistent with earlier studies which showed the involvement of a vanadate-sensitive P-type ATPase in creating H^+ extrusion areas (Smith 1988, Mimura et al. 1993, Badger and Price 1994, Ray et al. 2003). So far, a characean P-type ATPase has been biochemically characterized only in one study in which an antibody from Arabidopsis recognized a 140 kDa polypeptide in Western blots of the salt-tolerant *C. longifolia* (Faraday et al. 1996). Its molecular weight is higher than that measured for most proton pumps, suggesting the occurrence of several isoforms in plasma membranes of internodal cells.

In our study we were also able to stain the charasomes with the acidotropic dyes neutral red and Lysotracker red. This is evidence that the increase in plasma membrane influences transmembrane transport not only via simple multiplicative effects. Charasomes provide regions separated from the bulk medium by a convoluted diffusion path. H^+ exported to such regions will be slower to diffuse away and hence will be more effective in generating a locally low pH (Chau et al. 1994). This locally low pH increases the availability for CO_2 which results in enhanced photosynthesis as compared with the alkaline regions (see the Introduction). In addition, acidic regions

(charasomes) appear to be involved in Cl^- uptake (Beilby and Walker 1981, Keifer et al. 1982, Lucas et al. 1986).

There are several reports on the occurrence of similar membrane structures in higher plant cells that are produced by the elaboration of plasma membrane areas and which have been called plasmalemmasomes (Robinson et al. 1998, and references therein). Their physiological role has remained elusive, although roles in endocytosis, exocytosis and transport have been proposed (Robinson et al. 1998, Meyer et al. 2009). In epidermal cells of aquatic angiosperms an increase in plasma membrane surface is achieved by cell wall ingrowths. These regions are supposed to be involved in the acidification of the environment and may increase the efficiency of HCO_3^- utilization (Prins et al. 1982). An increase in plasma membrane surface along cell wall ingrowths is also typical for transfer cells which are specialized in transport of solutes and metabolites (Offler et al. 2003), and the underlying plasma membrane has been reported to be heavily labeled by an antibody against H^+-ATPase (Bouche-Pillon et al. 1994). All these data suggest that charasomes are morphologically and functionally related to plasma membrane infoldings in higher plant cells. In contrast to those, characean internodal cells are not embedded in a tissue and are easily accessible. This and the fact that fluorescent plasma membrane stains can now be used for in vivo observation of charasomes make characean internodal cells a promising system for studying developmental and transport processes associated with plasma membrane elaborations.

Photosynthesis-dependent pH banding required for differential distribution of charasomes

It is known that charasomes disappear through prolonged inhibition of photosynthesis by drugs or darkness (Bisson et al. 1991, Chau et al. 1993). The results of these EM studies are consistent with our findings about the effect of DCMU which resulted in a complete loss of FM-labeled patches after 10 d.

The DCMU-dependent degradation or inhibition of the development of charasomes could be an indirect effect of the arrest of pH banding. Indeed, cells incubated in BB supplemented with pH buffers at concentrations which inhibit pH banding had smaller and more homogeneously distributed charasomes than those incubated in BB alone. A complete loss of charasomes, however, was never observed, indicating that small charasomes can develop in the absence of pH banding as long as photosynthesis is not inhibited. Our experiments with pH-buffered solutions, containing 5 mM MES or TAPS, also rule out the possibility that the size and distribution of charasomes according to the pH banding pattern is caused by extreme differences in extracellular pH because the average size of charasomes was similar at pH 5.5 and pH 8.5. These results indicate that the pH-dependent size and differential distribution of charasomes requires or at least reflects active, photosynthesis-dependent pH banding.

In this study we used branchlet cells which were isolated from the thallus and then incubated in various solutions. We found that an acid pH of the BB (without MES or TAPS) favored the formation of larger charasomes at acid bands. In acid cultures, however, smaller charasomes have been reported (Price et al. 1985, Lucas et al. 1986). These differences are probably due to the use of different carbon sources. During our experiments cells were covered by a thin layer of medium only, and were therefore well supplied with CO_2 from the air environment. In culture experiments, diffusion of CO_2 into the culture medium was either prevented by a paraffin layer (Lucas et al. 1986) or cultures were kept at a specific CO_2/HCO_3^- equilibrium (Price et al. 1985) so that cells had to use bicarbonate. These data may indicate that acid pH of the medium promotes charasome development when CO_2 is available in sufficient amounts and that alkaline pH promotes charasome development when HCO_3^- is used as carbon source (for further discussion see Price et al. 1985). Here we investigated the differences in charasome size, density and area fraction between (the previously) acid and alkaline regions. Work is now in progress to study the distribution of charasomes along the whole cell surface. This will lead to a deeper insight into the formation of charasomes and their significance for ion transport and photosynthesis.

Interactions of cortical organelles

Together with an increased availability of carbon, acid bands feature enhanced photosynthesis, indicated through higher PSII activity and brighter Chl fluorescence, compared with alkaline regions (Plieth et al. 1994, Bulychev et al. 2001a, Bulychev and Vredenberg 2003). An intimate association of charasomes with subjacent chloroplasts has already been reported by Franceschi and Lucas (1980) and could also be observed in this study, indicating a close collaboration in energy metabolism. The third member in this metabolic unit are cortical mitochondria, which are significantly larger and more frequent within the highly photosynthetic active, acid regions (see also Foissner 2004). They are not only less abundant and smaller in alkaline regions, but are also more weakly stained with Mitotracker orange, indicating lower membrane potential and thus lower activity (Scorrano et al. 1999). Intimate contacts between mitochondria and chloroplasts have frequently been described (Logan and Leaver 2000). Mitochondrial metabolism is essential not only for photosynthetic carbon assimilation, but also for protection of chloroplasts against reactive oxygen species, arising during photosynthesis (Padmasree et al. 2002). The stationary chloroplasts in characean internodes are not able to escape high light intensities by light-dependent movement (Wada et al. 2003), and the accumulation of mitochondria in regions with high rates of photosynthesis may therefore be an alternative strategy against photodamage (Foissner 2004). In higher plant cells, peroxisomes—in addition to mitochondria—participate in detoxification of chloroplast-derived metabolites (Padmasree et al. 2002). Further studies are now in progress to clarify their role in photosynthesis of characean internodal cells.

Materials and Methods

Plant material and inhibitor experiments

Shoot tips of *C. corallina* Klein ex Willd. Em. R.D.W., *C. braunii* Gm. and *N. pseudoflabellata* A.Br., em. R.D.W. were planted in an about 5 cm high layer of a soil–peat–sand mixture which covered the bottom of an aquarium or a plastic bucket and which was filled with distilled water. Fluorescence lamps provided a 16/8 h light and dark cycle. After growth for 4 weeks at a temperature of about 20°C young but non-elongating internodes of branchlets were used for the experiments and isolated from the main axis with a small pair of scissors. Unless otherwise stated, branchlets were incubated in BB (2.0 mM $NaHCO_3$, 0.3 mM $CaCl_2$, 1.0 mM NaCl, 0.1 mM KCl; pH 8.4) at least 1 d prior to experiments to induce banding activity and to exclude unspecific stress response.

The effect of external pH was studied in cells incubated in BB supplemented by 5 mM MES (pH 5.5), HEPES (pH 7; data not shown) and TAPS (pH 8.5; all buffers from Sigma). Photosynthesis was inhibited by 10 μM DCMU (Serva), which affects PSII. The 10 mM stock solution in ethanol was diluted with BB and control cells were incubated in BB. Solutions were exchanged every second day. All experiments were performed at room temperature in small Petri dishes or in wells of microtiter plates with a diameter of 3.5 cm and a solution volume of 2 ml. Fluorescent lamps provided a quantum flux of 5 $\mu E\ m^{-2}\ s^{-1}$ at the surface of the Petri dishes and a 16/8 h light and dark cycle.

Banding pattern

The ability of internodal cells to form acid and alkaline bands was visualized using the pH indicator dye phenol red (phenolsulfonphthalein; Sigma). With a visual transition interval of 6.8–8.2 phenol red can be used to detect large differences in pH in the medium around the cells (Spear et al. 1969). Isolated branchlets were placed in a Petri dish filled with 10 mM phenol red in BB and exposed to direct sunlight for several minutes to initiate banding activity. Once banding occurred, cells were photographed with a Canon EOS 30D digital SLR camera (Canon, Vienna, Austria), equipped with an SP AF 90 mm F/2.8 Di macro zoom lens (Tamron). After mapping the banding pattern, these cells were incubated in BB for further investigations.

In vivo staining

The plasma membrane of lateral internodes was stained with different fluorescent probes. The FM dyes FM 4-64 (*N*-[3-triethylammoniumpropyl]-4-{6-[4-(diethylamino) phenyl] hexatrienyl}-pyridinium dibromide; Invitrogen; stock solution 0.5 mM in H_2Obidest) and the fixable analog of FM 1-43 fx [*N*-(3-triethylammoniumpropyl)-4-(dibutylamino)styryl pyridinium dibromide; Invitrogen; stock solution 0.5 mM in H_2O] were used at a concentration of 10 μM in BB. NBD C_6-sphingomyelin (6-{[*N*-(7-nitrobenz-2-oxa-1,3-diazol-4-yl)amino]hexanoyl}sphingosyl phosphocholine; Invitrogen; stock solution 1 mM in dimethylsulfoxide (DMSO)) was diluted to 10 μM in BB. A stock solution of filipin III (Sigma; 25 $mg\ ml^{-1}$ in DMSO) was diluted 1 : 4,000 in BB. In order to stain acidic compartments, internodal cells were incubated in the presence of 17 μM neutral red (Merck; stock solution 34 mM in H_2O) or 10 μM Lysotracker red DND-99 (Invitrogen; stock solution 1 mM in DMSO), respectively. Stock solutions were diluted with AFW (0.1 mM $CaCl_2$, 1 mM NaCl, 0.1 mM KCl; pH 5.5). Cells were loaded with neutral red and Lysotracker red for at least 12 h under low light conditions at room temperature. Mitochondria were fluorescently labeled by addition of Mitotracker orange CMTM Ros (Invitrogen; stock solution 1 mM in DMSO) to BB to a final concentration of 1 μM. An incubation time of 30 min was sufficient for brightly fluorescent mitochondria.

Internodal cells of the same culture and of similar age were used as controls and treated with the corresponding amounts of solvent, which never exceeded 1% DMSO or 0.1% acetone, respectively. These concentrations had no visible effect on cytoplasmic streaming or internalization of dyes.

After staining, cells were mounted either in BB for FM dyes, NBD C_6-sphingomyelin, filipin and Mitotracker, or in AFW for the acidotropic dyes neutral red and Lysotracker red on the coverslip bottom of perfusion chambers and topped with a coverslip fragment supported by sufficient vaseline at its corner to ensure a distance of at least 0.5 mm. To correlate the distribution of cortical organelles with pH banding, the coverslip bottom was marked according to the previously mapped banding pattern.

Immunofluorescence

Modified fixation and staining protocols described by Wasteneys and Williamson (1987) were used for indirect immunofluorescence of the plasma membrane proton pump.

For co-localization of the plasma membrane proton pump with plasma membrane patches, cells were stained with FM 1-43 fx and fixed with 1% (v/v) glutaraldehyde in phosphate-buffered saline (PBS; 140 mM NaCl, 2.95 mM KCl, 2.38 mM KH_2PO_4, 7.61 mM Na_2HPO_4, 18.5 mM NaN_3; pH 6.9) for 30 min at room temperature. Cells were dissected with a small pair of scissors and fragments were further treated as follows: 15 min wash with PBS, 3 × 15 min wash with PBS, 30 min treatment with 1 $mg\ ml^{-1}$ $NaBH_4$ in PBS, 3 × 15 min wash with PBS, 30 min blocking with 1% (w/v) bovine serum albumin (BSA) and 50 mM glycine in PBS, 2 h incubation with primary antibody in 1% (w/v) BSA and 50 mM glycine in PBS, 3 × 30 min wash with PBS, overnight incubation with secondary antibody in 1% (w/v) BSA and 50 mM glycine in PBS at 4°C, 3 × 30 min wash with PBS. Unless otherwise stated, all incubation steps were performed at room temperature. After the final wash cell fragments were mounted in PBS.

An IgG antibody raised in rabbit against a synthetic peptide derived from available plant, fern, moss and algal plasma membrane ATPase sequences (AS07260; Agrisera) was used at a

dilution of 1:200 and combined with an Alexa Fluor 546-conjugated anti-rabbit IgG produced in goat (A11010; Invitrogen) and diluted 1:1,000. Rabbit pre-immune serum (Sigma) at the same concentration as the primary antibody was used as negative control.

Confocal laser scanning microscopy (CLSM)

Fluorescent material was visualized by CLSM using either a Zeiss Axiovert 100 M inverted microscope (Zeiss), coupled to a Zeiss LSM 510 confocal laser scanner or a Leica TCS SP5 AOBS confocal laser scanning system (Leica Microsystem) coupled to a Leica DMI 6000 Cs inverted microscope, both equipped with differential interference contrast (DIC) optics. Settings for excitation (ex) and detection of emission (em) were chosen as follows: FM 1-43, NBD C_6-sphingomyelin and Alexa 488 (ex 488 nm; em 505–530 or 520–570 nm); Mitotracker orange, neutral red, Lysotracker red and Nile red (ex 543 nm; em 560–615 nm); FM 4-64 (ex 514 nm; em 570–600 nm); Alexa 546 (ex 561 nm; em 570–600 nm); filipin (ex 375 nm; em 450–500 nm); Chl (ex 488 nm; em >585 nm or 600–700 nm). Sequential line scan modus (multitracking) was used in order to decrease further cross-talk of double-stained samples. Stacks of five serial confocal sections (Z-series) were taken for average intensity projections, generated by the Zeiss LSM 510 or Leica LAS AF software. Images of cells are positioned with horizontal sides parallel to the long axes of the internodes. Further image processing was done by ImageJ (National Institutes of Health, Bethesda, MD; http://rsb.info.nih.gov/ij) and Adobe Photoshop (Adobe Systems Inc.).

Image analysis and statistics

ImageJ was used to count and measure plasma membrane domains, cortical mitochondria and autofluorescent chloroplasts. Parametric and non-parametric tests were performed with SigmaStat (Systat Software, Erkrath, Germany; version 3.11) in order to reveal significant differences ($P \leq 0.05$) in size (given as the largest cross-section or diameter), numerical density (number of organelles per unit cortical area) and area fraction (percentage of cortical area occupied by organelles) between acid and alkaline bands. Bar charts as well as box and line plots were generated with SigmaPlot (Systat Software; version 9.01).

Protein extraction, SDS–PAGE and Western blot analysis

Whole thalli of *C. corallina* were harvested, washed in BB, briefly blotted dry, weighed and frozen in liquid nitrogen. After homogenization with a pestle and mortar, the homogenate was resuspended in ice-cold extraction buffer [330 mM saccharose, 100 mM KCl, 1 mM EDTA, 50 mM Tris–HCl pH 7.4, 0.5 mM phenylmethylsulfonyl fluoride (PMSF), 5 mM dithiothreitol (DTT) and 1% (v/v) protease inhibitor cocktail (P9599; Sigma)] at a ratio of 0.5 ml g FW^{-1}. Cell debris was removed by centrifugation at 8,000 × *g* for 10 min at 4°C. The supernatant was again centrifuged at 100,000 × g for 1 h at 4°C and the resulting supernatant, representing the cytosolic fraction (CF) was aliquoted, frozen in liquid nitrogen and stored at −80°C. The pellet was resuspended in extraction buffer (microsomal fraction; MF) before being frozen and stored. The protein concentration was determined using Roti-Nanoquant (Roth).

Protein extracts were separated on a 10% SDS gel according to Laemmli (1970) using a Mini-PROTEAN III electrophoresis system (BioRad) and stained with aluminium sulfate–Coomassie (Dyballa and Metzger 2009).

For Western blots, proteins were transferred to a polyvinylidene fluoride (PVDF) membrane (Millipore) using a Mini Trans-Blot Cell (BioRad). Blots were blocked with 1% (w/v) BSA in Tris-buffered saline with Tween [TBST; 13 mM Tris, 150 mM NaCl, 0.1% (w/v) Tween-20] for 1 h and incubated overnight at 4°C with anti-H^+-ATPase diluted 1:1,000 in blocking solution. After washing in TBST (3 × 15 min), blots were incubated with a horseradish peroxidase-conjugated anti-rabbit IgG (A9169; Sigma) diluted 1:80,000 in blocking solution for 2 h and washed again in TBST. All incubation steps were performed at room temperature. Immunolabeled proteins were detected by enhanced chemiluminescence using a NOWA kit (MoBiTec) and an LAS-3000 mini lumiscent image analysis system (Fujifilm).

Electron microscopy

Lateral internodal cells of *C. braunii* were cryofixed in a Leica EMPACT high pressure freezer (Leica Microsystems), freeze-substituted in a Leica EM AFS freeze-substitution apparatus as described in Lütz-Meindl and Aichinger (2004) and were embedded in LR Gold Resin (London Resin Co.). Ultrathin sections with a maximum thickness of 80 nm were cut on a Reichert Ultracut E and were mounted on formvar-coated nickel grids. For immunolabeling, the sections were blocked in 0.05 M Trizma (Sigma) containing 1% (w/v) BSA and 0.1% (w/v) Tween-20 at room temperature for 30 min. The primary antibody against H^+-ATPase (AS07260; Agrisera) was used at a dilution of 1:25 in blocking solution; rabbit pre-immune serum at the same dilution was used as negative control. The incubation was carried out on 20 µl droplets at 6°C in a moist chamber for about 20 h. After washing four times (10 min) on 20 µl droplets of blocking solution, the secondary antibody, a 10 nm gold-conjugated anti-rabbit IgG produced in goat (G7402; Sigma) or a 15 nm gold-conjugated anti-rabbit IgG also produced in goat (EM.GAR15; British Biocell International), diluted 1:40 in blocking solution, was applied for 1 h at room temperature. Thereafter, the grids were washed in blocking solution, and finally rinsed with ddH_2O.

Micrographs at elastic bright-field mode were taken with a LEO 912 transmission electron microscope (Zeiss) equipped with an in-column energy filter. The electron microscope was operated with a LaB_6 cathode at 80 kV. A Slow Scan Dual Speed CCD camera TRS Sharpeye (Troendle) controlled by ITEM software (SIS, Soft Image System) was used for image acquisition.

Supplementary data

Supplementary data are available at PCP online.

Funding

This research was funded by the Austrian Science Fund (FWF): project No. P 22957-B20.

Acknowledgments

We thank Anja Geretschläger, Marion Höpflinger, Aniela Sommer (University of Salzburg), Sebastien Mongrand (CNRS, Université de Bordeaux) and Markus Grebe (Umeå Plant Science Centre) for critical reading and valuable discussion.

References

Badger, M.R. and Price, G.D. (1994) The role of carbonic-anhydrase in photosynthesis. *Annu. Rev. Plant Physiol. Plant Mol. Biol.* 45: 369–392.

Barton, R. (1965a) Electron microscope studies on surface activity in cells of *Chara vulgaris*. *Planta* 66: 95–105.

Barton, R. (1965b) An unusual organelle in the peripheral cytoplasm of *Chara* cells. *Nature* 205: 201.

Beilby, M.J. and Walker, N.A. (1981) Chloride transport in *Chara*. 1. Kinetics and current–voltage curves for a probable proton symport. *J. Exp. Bot.* 32: 43–54.

Betz, W.J., Mao, F. and Smith, C.B. (1996) Imaging exocytosis and endocytosis. *Curr. Opin. Neurobiol.* 6: 365–371.

Bisson, M.A., Siegel, A., Chau, R., Gelsomino, S.A. and Herdic, S.L. (1991) Distribution of charasomes in *Chara*—banding-pattern and effect of photosynthetic inhibitors. *Aust. J. Plant Physiol.* 18: 81–93.

Bolte, S., Talbot, C., Boutte, Y., Catrice, O., Read, N.D. and Satiat-Jeunemaitre, A. (2004) FM-dyes as experimental probes for dissecting vesicle trafficking in living plant cells. *J. Microsc.* 214: 159–173.

Bouche-Pillon, S., Fleurat-Lessard, P., Fromont, J.C., Serrano, R. and Bonnemain, J.L. (1994) Immunolocalization of the plasma membrane H^+-ATPase in minor veins of *Vicia faba* in relation to phloem loading. *Plant Physiol.* 105: 691–697.

Bulychev, A. and Vredenberg, W. (2003) Spatio-temporal patterns of photosystem II activity and plasma-membrane proton flows in *Chara corallina* cells exposed to overall and local illumination. *Planta* 218: 143–151.

Bulychev, A.A., Cherkashin, A.A., Rubin, A.B., Vredenberg, W.J., Zykov, V.S. and Müller, S.C. (2001a) Comparative study on photosynthetic activity of chloroplasts in acid and alkaline zones of *Chara corallina*. *Bioelectrochemistry* 53: 225–232.

Bulychev, A.A., Polezhaev, A.A., Zykov, S.V., Pljusnina, T.Y., Riznichenko, G.Y., Rubin, A.B. et al. (2001b) Light-triggered pH banding profile in *Chara* cells revealed with a scanning pH microprobe and its relation to self-organization phenomena. *J. Theor. Biol.* 212: 275–294.

Campbell, A.M., Coble, A.J., Cohen, L.D., Ch'Ng, T.H., Russo, K.M., Long, E.M. et al. (2001) Identification and DNA sequence of a new H^+-ATPase in the unicellular green alga *Chlamydomonas reinhardtii* (Chlorophyceae). *J. Phycol.* 37: 536–542.

Chau, R., Bisson, M.A., Siegel, A., Elkin, G., Klim, P. and Straubinger, R.M. (1994) Distribution of charasomes in *Chara*—reestablishment and loss in darkness and correlation with banding and inorganic carbon uptake. *Aust. J. Plant Physiol.* 21: 113–123.

Crawley, J.C.W. (1965) A cytoplasmic organelle associated with the cell walls of *Chara* and *Nitella*. *Nature* 205: 200–201.

Diwu, Z., Zhang, Y. and Haugland, R.P. (1994) Novel site-selective fluorescent probes for lysosome and acidic organelle staining and long-term tracking. *Cytometry* 18: 77; (abstract 426b).

Duby, G. and Boutry, M. (2008) The plant plasma membrane proton pump ATPase: a highly regulated P-type ATPase with multiple physiological roles. *Pflugers Arch.* 457: 645–655.

Dubrovsky, J.G., Guttenberger, M., Saralegui, A., Napsucialy-Mendivil, S., Voigt, B., Baluska, F. et al. (2006) Neutral red as a probe for confocal laser scanning microscopy studies of plant roots. *Ann. Bot.* 97: 1127–1138.

Dyballa, N. and Metzger, S. (2009) Fast and sensitive colloidal coomassie G-250 staining for proteins in polyacrylamide gels. *J. Vis. Exp.* 30: e1431.

Faraday, C.D., Spanswick, R.M. and Bisson, M.A. (1996) Plasma membrane isolation from freshwater and salt-tolerant species of *Chara*: antibody cross-reactions and phosphohydrolase activities. *J. Exp. Bot.* 47: 589–594.

Ferrier, J.M. (1980) Apparent bicarbonate uptake and possible plasmalemma proton efflux in *Chara corallina*. *Plant Physiol.* 66: 1198–1199.

Fisahn, J. and Lucas, W.J. (1990) Application of asymmetric alternating voltage pulse series for investigation of the action-potential in *Chara*. *Plant Cell Physiol.* 31: 155–157.

Foissner, I. (2004) Microfilaments and microtubules control the shape, motility, and subcellular distribution of cortical mitochondria in characean internodal cells. *Protoplasma* 224: 145–157.

Foissner, I. and Klima, A. (2008) Constitutive endocytosis in characean internodal cells is independent of an intact actin cytoskeleton. *Cell Biol. Int.* 32: 579–580.

Franceschi, V.R. and Lucas, W.J. (1980) Structure and possible function(s) of charasomes; complex plasmalemma–cell wall elaborations present in some characean species. *Protoplasma* 104: 253–271.

Franceschi, V.R. and Lucas, W.J. (1982) The relationship of the charasome to chloride uptake in *Chara corallina*: physiological and histochemical investigations. *Planta* 154: 525–537.

Grabski, S., De Feijter, A.W. and Schindler, M. (1993) Endoplasmic reticulum forms a dynamic continuum for lipid diffusion between contiguous soybean root cells. *Plant Cell* 5: 25–38.

Grebe, M., Xu, J., Mobius, W., Ueda, T., Nakano, A., Geuze, H.J. et al. (2003) Arabidopsis sterol endocytosis involves actin-mediated trafficking via ARA6-positive early endosomes. *Curr. Biol.* 13: 1378–1387.

Harper, J.F., Surowy, T.K. and Sussman, M.R. (1989) Molecular cloning and sequence of cDNA encoding the plasma membrane proton pump (H^+-ATPase) of *Arabidopsis thaliana*. *Proc. Natl Acad. Sci. USA* 86: 1234–1238.

Keifer, D.W., Franceschi, V.R. and Lucas, W.J. (1982) Plasmalemma chloride transport in *Chara corallina*—inhibition by 4,4′-diisothiocyano-2,2′-disulfonic acid stilbene. *Plant Physiol.* 70: 1327–1334.

Klima, A. and Foissner, I. (2008) FM dyes label sterol-rich plasma membrane domains and are internalized independently of the cytoskeleton in characean internodal cells. *Plant Cell Physiol.* 49: 1508–1521.

Laemmli, U.K. (1970) Cleavage of structural proteins during the assembly of the head of bacteriophage T4. *Nature* 227: 680–685.

Logan, D.C. and Leaver, C.J. (2000) Mitochondria-targeted GFP highlights the heterogeneity of mitochondrial shape, size and movement within living plant cells. *J. Exp. Bot.* 51: 865–871.

Lucas, W.J. (1983) Photosynthetic assimilation of exogenous HCO_3^- by aquatic plants. *Annu. Rev. Plant Physiol.* 34: 71–104.

Lucas, W.J., Brechignac, F., Mimura, T. and Oross, J.W. (1989) Charasomes are not essential for photosynthetic utilization of exogenous HCO_3^- in *Chara corallina*. *Protoplasma* 151: 106–114.

Lucas, W.J. and Dainty, J. (1977) Spatial distribution of functional OH^- carriers along a characean internodal cell: determined by the effect of cytochalasin B on $H^{14}CO_3$ assimilation. *J. Membr. Biol.* 32: 75–94.

Lucas, W.J. and Franceschi, V.R. (1981) Characean charasome-complex and plasmalemma vesicle development. *Protoplasma* 107: 255–267.

Lucas, W.J., Keifer, D.W. and Pesacreta, T.C. (1986) Influence of culture-medium pH on charasome development and chloride transport in *Chara corallina*. *Protoplasma* 130: 5–11.

Lucas, W.J. and Smith, F.A. (1973) The formation of alkaline and acid regions at the surface of *Chara corallina* cells. *J. Exp. Bot.* 24: 1–14.

Lütz-Meindl, U. and Aichinger, N. (2004) Use of energy-filtering transmission electron microscopy for routine ultrastructural analysis of high-pressure-frozen or chemically fixed plant cells. *Protoplasma* 223: 155–162.

McConnaughey, T.A. and Falk, R.H. (1991) Calcium–proton exchange during algal calcification. *Biol. Bull.* 180: 185–195.

Meyer, D., Pajonk, S., Micali, C., O'Connell, R. and Schulze-Lefert, P. (2009) Extracellular transport and integration of plant secretory proteins into pathogen-induced cell wall compartments. *Plant J.* 57: 986–999.

Mimura, T. (1995) Physiological characteristics and regulation mechanisms of the H^+ pumps in the plasma membrane and tonoplast of characean cells. *J. Plant Res.* 108: 249–256.

Mimura, T., Müller, R., Kaiser, W.M., Shimmen, T. and Dietz, K.J. (1993) ATP-dependent carbon transport in perfused *Chara* cells. *Plant Cell Environ.* 16: 653–661.

Mongrand, S., Morel, J., Laroche, J., Claverol, S., Carde, J.P., Hartmann, M.A. et al. (2004) Lipid rafts in higher plant cells—purification and characterization of triton X-100-insoluble microdomains from tobacco plasma membrane. *J. Biol. Chem.* 279: 36277–36286.

Offler, C.E., McCurdy, D.W., Patrick, J.W. and Talbot, M.J. (2003) Transfer cells: cells specialized for a special purpose. *Annu. Rev. Plant Biol.* 54: 431–454.

Padmasree, K., Padmavathi, L. and Raghavendra, A.S. (2002) Essentiality of mitochondrial oxidative metabolism for photosynthesis: optimization of carbon assimilation and protection against photoinhibition. *Crit. Rev. Biochem. Mol. Biol.* 37: 71–119.

Plieth, C., Tabrizi, H. and Hansen, U.P. (1994) Relationship between banding and photosynthetic activity in *Chara corallina* as studied by spatially different induction curves of chlorophyll fluorescene observed by an image analysis system. *Physiol. Plant.* 91: 205–211.

Price, G.D. and Whitecross, M.I. (1983) Cytochemical localisation of ATPase activity on the plasmalemma of *Chara corallina*. *Protoplasma* 116: 65–74.

Price, G.D., Badger, M.R., Bassett, M.E. and Whitecross, M.I. (1985) Involvement of plasmalemmasomes and carbonic anhydrase in photosynthetic utilization of bicarbonate in *Chara corallina*. *Aust. J. Plant Physiol.* 12: 241–256.

Prins, H.B.A., Snel, H., Zanstra, P.E. and Helder, R.J. (1982) The mechanism of bicarbonate assimilation by the polar leaves of *Potamogeton* and *Elodea*. CO_2 concentrations at the leaf surface. *Plant Cell Environ.* 5: 207–214.

Raffaele, S., Bayer, E., Lafarge, D., Cluzet, S., German Retana, S., Boubekeur, T. et al. (2009) Remorin, a solanaceae protein resident in membrane rafts and plasmodesmata, impairs potato virus X movement. *Plant Cell* 21: 1541–1555.

Ray, S., Klenell, M., Choo, K.S., Pedersen, M. and Snoeijs, P. (2003) Carbon acquisition mechanisms in *Chara tomentosa*. *Aquat. Bot.* 76: 141–154.

Robinson, D.G., Galili, G., Herman, E. and Hillmer, S. (1998) Topical aspects of vacuolar protein transport: autophagy and prevacuolar compartments. *J. Exp. Bot.* 49: 1263–1270.

Robinson, J.M. and Karnovsky, M.J. (1980) Evaluation of the polyene antibiotic filipin as a cytochemical probe for membrane cholesterol. *J. Histochem. Cytochem.* 28: 161–168.

Schulte, C., Kirst, G.O and Winter, U. (1994) Source–sink characteristic of photoassimilate transport in fertile and sterile plants of *Chara vulgaris* L. *Bot. Acta* 107: 362–368.

Scorrano, L., Petronilli, V., Colonna, R., Di Lisa, F. and Bernardi, P. (1999) Chloromethyltetramethylrosamine (Mitotracker Orange^{TM}) induces the mitochondrial permeability transition and inhibits respiratory complex I. Implications for the mechanism of cytochrome c release. *J. Biol. Chem.* 274: 24657–24663.

Smith, F.A. and Walker, N.A. (1980) Effects of ammonia and methylamine on Cl^- transport and on the pH changes and circulating electric currents associated with HCO_3^- assimilation in *Chara corallina*. *J. Exp. Bot.* 31: 119–133.

Smith, R.G. (1988) Inorganic carbon transport in biological systems. *Comp. Biochem. Physiol. Biochem. Mol. Biol.* 90: 639–654.

Spanswick, R.M. (1981) Electrogenic ion pumps. *Annu. Rev. Plant Physiol. Plant Mol. Biol.* 32: 267–289.

Spear, D.G., Barr, J.K. and Barr, C.E. (1969) Localization of hydrogen ion and chloride ion fluxes in *Nitella*. *J. Gen. Physiol.* 54: 397–414.

Tazawa, M. (2003) Plant plasma membrane H^+ pumps: past and present. *J. Plant Res.* 116: 399–400.

Tazawa, M. and Shimmen, T. (2001) How characean cells have contributed to the progress of plant membrane biophysics. *Aust. J. Plant Physiol.* 28: 523–539.

Wada, M., Kagawa, T. and Sato, Y. (2003) Chloroplast movement. *Annu. Rev. Plant Biol.* 54: 455–468.

Walker, N.A., Smith, F.A. and Cathers, I.R. (1980) Bicarbonate assimilation by freshwater charophytes and higher-plants. 1. Membrane-transport of bicarbonate ions is not proven. *J. Membr. Biol.* 57: 51–58.

Wasteneys, G.O. and Williamson, R.E. (1987) Microtubule orientation in developing internodal cells of *Nitella*—a quantitative-analysis. *Eur. J. Cell Biol.* 43: 14–22.

Wood, R.D. and Imahori, K. (1965) *In* Monograph of the Characeae. Cramer, Weinheim.

Zhang, Y.-Z., Olwu, Z., Mao, F., Leung, W. and Haugland, R.P. (1994) Novel fluorescent acidic organelle-selective dyes and mitochondrion-selective dyes that are well retained during cell fixation and permeabilization. *Mol. Biol. Cell* 5: 113a; (abstract 653).